SynHydro: Biomechanics-Driven Domain Randomization for Hydrocephalus-Agnostic, Generalizable Tissue-Ventricle Segmentation Across Age, Modality, and Resolution

Zehua Ren[1,4⋆], Jingyan Zhai[2,4*], Haifeng Wang[3,4], Yixuan Bo[5], Fan Wang[1,4], Cailei Zhao[6,(✉)], and Chunfeng Lian[3,4,(✉)]

[1] Key Laboratory of Biomedical Information Engineering of Ministry of Education, School of Life Science and Technology, Xi'an Jiaotong University, Xi'an, China
[2] School of Software Engineering, Xi'an Jiaotong University, Xi'an, China
[3] School of Mathematics and Statistics, Xi'an Jiaotong University, Xi'an, China
[4] Research Center for Intelligent Medical Equipment and Devices (IMED), Xi'an Jiaotong University, Xi'an, China
[5] Shenzhen University, Shenzhen, China
[6] Shenzhen Children's Hospital, Shenzhen, China
zhaocailei197866@163.com; chunfeng.lian@xjtu.edu.cn

Abstract. Early diagnosis and quantitative assessment of pediatric hydrocephalus are critical, yet automated segmentation remains challenging due to severe anatomical deformation and substantial appearance variation across early neurodevelopment, imaging modalities, and resolutions. Current deep learning approaches are often limited to ventricle-only segmentation and tailored to specific acquisition protocols, hindering their clinical utility for comprehensive joint tissue analysis and longitudinal evaluation. We propose **SynHydro**, a novel biomechanics-driven simulation and domain-randomized augmentation framework. SynHydro synthesizes diverse hydrocephalus anatomies from readily available healthy tissue labels and generates corresponding MRIs with randomized image characteristics. This creates a large-scale, synthetic training dataset encompassing a wide spectrum of disease severity, MRI contrast, noise, resolution, and artifacts for joint tissue-ventricle segmentation. Extensive experiments on in-house and public datasets demonstrate that a segmentation model trained exclusively on this pure synthetic data achieves performance comparable to models trained with real hydrocephalus annotations. More importantly, SynHydro-trained models exhibit superior cross-modality and cross-resolution robustness, and reliably preserve pre-/post-operative volumetric trends. By eliminating the dependency on labor-intensive pathological annotations, SynHydro provides a powerful and practical solution for building robust, generalizable segmentation tools for pediatric hydrocephalus monitoring across the clinical imaging landscape. Code is available at https://github.com/ladderlab-xjtu/SynHydro.

⋆ These authors contributed equally.

Keywords: Pediatric Hydrocephalus · Data Simulation · Domain Randomization · Biomechanics-Driven · Tissue-Ventricle Segmentation.

1 Introduction

Hydrocephalus is a pathological condition characterized by the excessive accumulation of cerebrospinal fluid (CSF) within the cerebral ventricles, leading to progressive compression and deformation of the surrounding brain parenchyma [12,14,3]. In pediatric patients, this process unfolds during a period of rapid neurodevelopment, making timely diagnosis and quantitative monitoring critical for mitigating potential long-term neurological impairment [10,21,19]. Magnetic resonance imaging (MRI) serves as the primary modality for diagnosis and surgical follow-up, where clinicians rely on precise segmentation of both ventricles and brain tissues (gray and white matter) to assess disease severity and track longitudinal changes before and after intervention [25,16].

The development of automated segmentation tools for this task, however, is confronted with significant challenges stemming from the unique characteristics of pediatric hydrocephalus imaging: **(1) Extreme Anatomical Variability:** Massive ventricular enlargement causes severe compression and displacement of adjacent tissues, breaking the anatomical assumptions of standard neuroimaging pipelines [2,28,22,8,20,1]. **(2) Evolving Image Appearance:** The rapidly changing myelination patterns in the developing brain lead to low tissue contrast and potential intensity inversion, complicating intensity-based segmentation. **(3) Heterogeneous Clinical Acquisitions:** Routine clinical scans vary widely in modality (T1w, T2w, FLAIR), resolution (3D, 2D), and quality (noise, artifacts), demanding exceptional model robustness.

Existing deep learning methodologies have made progress but remain limited. They are predominantly tailored to hydrocephalic scans and are mostly limited to ventricle-only segmentation [9,27,15,11,13]. Moreover, they are often developed under modality-specific assumptions, focusing on a single acquisition such as 3D T1-weighted (T1w) MRI [9,18], T2-weighted (T2w) MRI [13], ultrasound [23], or computed tomography (CT) [26,11]. Consequently, these models lack the generalizability for joint tissue-ventricle analysis across the diverse and often suboptimal imaging conditions encountered in real-world clinical practice.

To bridge this gap, we introduce SynHydro, an end-to-end biomechanics-driven simulation and domain randomization framework for robust, hydrocephalus-agnostic segmentation. Our core insight is to circumvent the scarcity of labor-intensive pathological annotations by synthesizing a comprehensive training dataset from readily available healthy tissue segmentations. The framework operates in three stages: first, a **biomechanical deformation module** synthesizes realistic hydrocephalus label maps of varying severity from healthy anatomies; second, a **domain-randomized image synthesis module** generates corresponding multi-contrast MRI with randomized image characteristics (contrast, noise, resolution, artifacts). At last, by training a standard nnU-Net [7] on this diverse synthetic cohort, which contains both normal and simulated pathological cases,

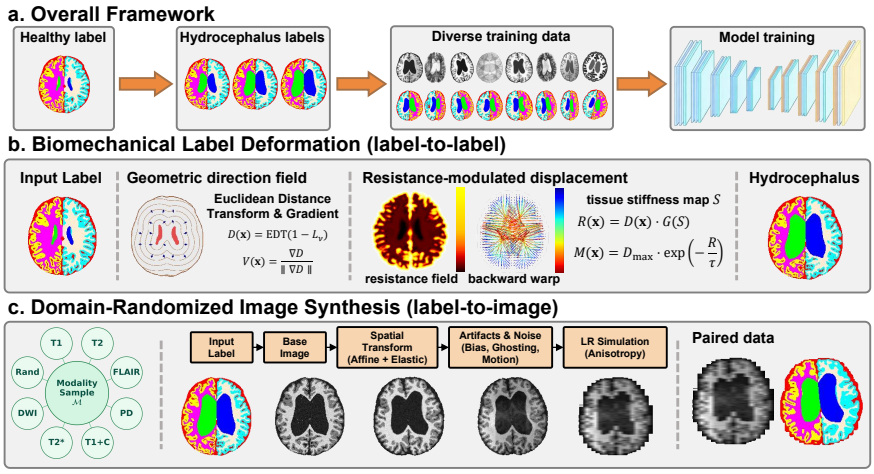

Fig. 1: **SynHydro pipeline.** From healthy labels, we simulate hydrocephalus via biomechanics-based label deformation, then synthesize multi-contrast images with acquisition randomization to train a robust segmentation model.

we obtain a single model that generalizes effectively across patient age, hydrocephalus severity, imaging modality, and resolution.

Extensive experiments on in-house longitudinal datasets and a public benchmark [24] demonstrate that a model trained purely on SynHydro-generated data achieves segmentation performance comparable to models trained with real hydrocephalus labels. More importantly, it exhibits superior cross-modality/cross-resolution robustness and faithfully preserves clinically relevant volumetric trends, such as pre-/post-operative changes.

2 Method

As shown in Fig. 1, **SynHydro** is an end-to-end simulation-to-training pipeline with three stages: **(1) Biomechanical Label Deformation** to synthesize hydrocephalus anatomy from healthy segmentations (label-to-label), **(2) Domain-Randomized Image Synthesis** to generate data pairs with varying conditions from the original and deformed labels (label-to-image), and **(3) Segmentation Training** on the resulting large-scale, synthetic paired data.

2.1 Biomechanical-Driven Hydrocephalus Anatomy Synthesis

We simulate ventricular enlargement directly in the *label space*, which is easier to control than image-space warping. The deformation is designed to satisfy key constraints: (i) skull-bounded brain extent (brain mask unchanged), (ii) topology preservation of nested tissue layout, (iii) tissue-dependent mechanics (different compressibility), and (iv) smooth and continuous deformation fields.

Based on these considerations, we propose a hydrocephalus simulation method driven by a continuous, resistance-modulated displacement field. Given a healthy label map L, with ventricle and brain mask L_v, L_b, the process is as follows:

Geometric direction field: To establish the foundational geometry for expansion, we compute the Euclidean Distance Transform (EDT) to determine the distance of each voxel to the closest ventricle boundary:

$$D(x) = \mathrm{EDT}(1 - L_v). \tag{1}$$

The simulated pressure exerts an outward force originating from the ventricles towards the brain boundary. This local expansion direction is defined by the normalized gradient of the distance field, yielding a continuous unit vector field:

$$\boldsymbol{V}(x) = \frac{\nabla D(x)}{\|\nabla D(x)\|}. \tag{2}$$

Resistance-modulated displacement: To model heterogeneous tissue response, we assign a tissue stiffness map $S(L(x))$ (shared across hemispheres for the same tissue) and smooth it to avoid boundary discontinuities. We then define an accumulated resistance field:

$$R(x) = D(x) \cdot \mathrm{Gaussian}(S(L(x)), \sigma). \tag{3}$$

The displacement magnitude decays with resistance:

$$M(x) = D_{\max} \cdot e^{-\frac{R(x)}{\tau}}, \tag{4}$$

where $D_{\max}$ controls hydrocephalus severity and τ controls attenuation. The final deformation field is smoothed and applied as a backward warp:

$$\phi(x) = x - \mathrm{Gaussian}(\boldsymbol{V}(x) \cdot M(x), \sigma_{\mathrm{smooth}}). \tag{5}$$

Warping L by ϕ yields a deformed label map with enlarged ventricles and compressed parenchyma while maintaining smoothness.

Ventricle filling and post-processing: Voxels newly occupied by CSF are determined by thresholding a resistance-based criterion and are assigned to left/right ventricles using nearest-label (Voronoi) assignment. We apply light morphological closing/opening to remove small holes and boundary artifacts, producing anatomically plausible contours. By sampling $D_{\max}$, τ, and stiffness/smoothing parameters, we generate multiple severities per healthy subject.

2.2 Domain-Randomized MRI Synthesis from Labels

Given a label map (original healthy or simulated hydrocephalus), we synthesize paired data with a domain-randomization strategy, following label-to-image paradigms [1,5,6,4] and extensively augmenting them to cover clinical heterogeneity.

Multi-contrast intensity sampling: We first sample a pseudo-modality $\mathcal{M}$ (e.g., T1/T2/FLAIR/PD/T2*/T1+C/DWI/random). For each tissue class k, Gaussian intensity parameters (μ_k, σ_k) are sampled from modality-specific ranges to generate the base image:

$$I_0(x) \sim \mathcal{N}(\mu_{L(x)}, \sigma^2_{L(x)}). \tag{6}$$

This exposes the model to diverse contrast variations and inversions seen during neurodevelopment.

Clinical degradations and resolution variation: The base image I_0 undergoes a series of stochastic transforms to emulate real-world acquisitions: random affine/elastic deformation, bias field, anisotropic blur, additive noise, and optional artifacts (e.g., motion, ghosting). To simulate thick-slice clinical scans, an axis is randomly selected, and the image is downsampled by a factor of 3-7 to create an anisotropic low-resolution (LR) volume.

2.3 Segmentation Model Training on Synthetic Data

Each label map is randomly re-synthesized multiple times to reach the target number of paired training samples. This yields a large, balanced training set containing both normal and varied hydrocephalus anatomies across a spectrum of modalities, resolutions, and artifacts. A 3D nnU-Net model is trained on this synthetic paired dataset.

3 Experimental Results

3.1 Dataset and Experimental Setting

Dataset and Preprocessing We evaluate our method on both in-house and external datasets to assess its performance and generalizability.

(i) In-house Pediatric Cohort that comprises a longitudinal and a control dataset for quantitative and qualitative evaluations. The longitudinal dataset includes 132 pre- and post-operative multi-modal MRI sessions (592 scans: 3D/2D T1w, T2w, FLAIR) from 35 pediatric hydrocephalus subjects (aged 2 months to 13 years). The control dataset consists of 131 multi-modal MRI scans from 44 healthy pediatric subjects (aged 1 month to 9 years). The 3D T1w scans were first segmented with iBEAT [22] and then refined by three radiologists to form the ground-truth labels. Voxels were labeled into 8 classes: background (0), extra-axial/lateral CSF (1), left/right ventricles (2/3), left/right GM (4/5), and left/right WM (6/7).

(ii) External Public Dataset (HyKid) [24] that contains 148 LR T1w scans from 48 pediatric hydrocephalus subjects (aged 0-17 years), for out-of-domain generalization testing. Notably, this dataset was used only for qualitative evaluation, considering that ground-truth labels consistent with the purpose of this study is not available.

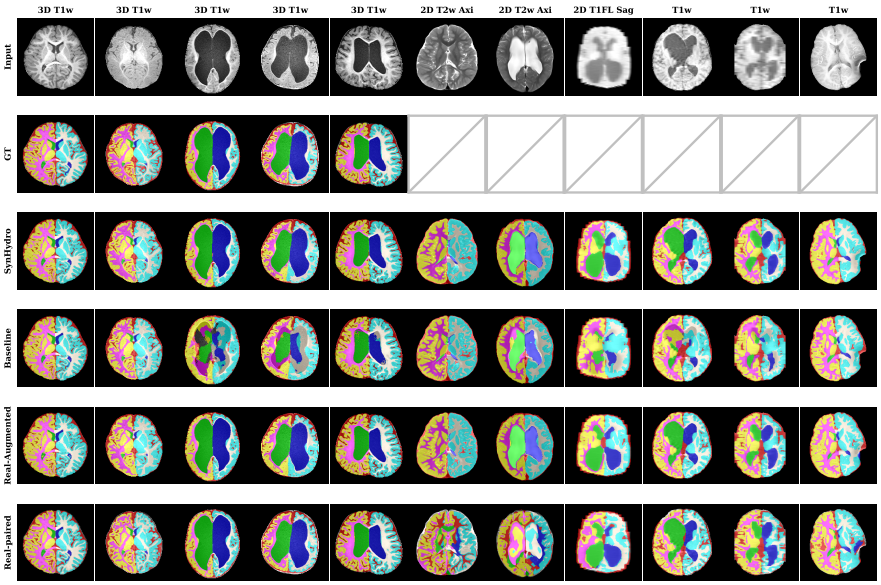

Fig. 2: Qualitative comparison across diverse input, covering control (Columns 1–2), longitudinal (Columns 3–8) and out-of-domain HyKid (Columns 9–11). For non-T1w and LR scans without manual annotations (Columns 6–11), the GT panels are left blank.

Implementations & Comparison Setting From the annotated 125 (longitudinal) and 47 (control) 3D T1w image-label pairs, We performed a subject-level split (65/60 for longitudinal, 35/12 for control) for training and testing.

Our SynHydro was implemented as follows: Healthy/control segmentations from the training split were fed into the biomechanical deformation module, sampling the $D_{\max}$ from 10–60 to generate 4 pseudo-hydrocephalus labels per case. Both original healthy and synthesized labels were then processed by the label-to-image module (implemented with TorchIO [17]) with extensive domain randomization. This yielded a final balanced training set of 1400 paired samples (700 hydrocephalus, 700 normal).

We evaluate SynHydro against three baselines: **(i) Baseline (Normal-Only)**: Trained solely on 1400 augmented data synthesized from 35 healthy control labels; **(ii) Real-Augmented**: Trained on 1400 augmented data synthesized from all available training labels (both longitudinal and control), representing a strong data-augmentation baseline with real pathological labels; **(iii) Real-paired**: Trained directly on all real 3D T1w image-label pairs, serving as an approximate performance upper bound for the in-domain T1w modality.

Table 1: **Geometric Evaluation Results.** Comparison of Dice Similarity Coefficient (DSC, ↑) on Control and Longitudinal cohorts. The Longitudinal dataset is divided into Pre-operative and Post-operative phases.

Dataset	Method	Anatomical Structure						Avg.
		Ven_L	Ven_R	GM_L	GM_R	WM_L	WM_R	
Control	Baseline	0.916	0.896	0.839	0.841	0.846	0.848	0.864
	SynHydro (Ours)	0.912	0.891	0.828	0.831	0.825	0.829	0.853
	Real-Augmented	0.899	0.890	0.828	0.832	0.819	0.826	0.849
	Real-Paired	0.948	0.932	0.888	0.891	0.879	0.880	0.903
Longitudinal *Pre-operative*	Baseline	0.623	0.598	0.780	0.787	0.654	0.661	0.684
	SynHydro (Ours)	0.960	0.964	0.811	0.826	0.798	0.814	0.862
	Real-Augmented	0.957	0.964	0.822	0.842	0.797	0.811	0.865
	Real-Paired	0.975	0.982	0.892	0.905	0.887	0.893	0.923
Longitudinal *Post-operative*	Baseline	0.735	0.719	0.847	0.833	0.819	0.813	0.794
	SynHydro (Ours)	0.873	0.874	0.853	0.838	0.853	0.845	0.856
	Real-Augmented	0.876	0.867	0.863	0.853	0.858	0.847	0.861
	Real-Paired	0.931	0.937	0.927	0.922	0.927	0.923	0.928

3.2 Quantitative and Qualitative Results

Qualitative Results Fig. 2 compares segmentation quality across diverse inputs from real scans, including w/o hydrocephalus cases with different ages, modalities, and resolutions. While all methods performed well on standard 3D T1w healthy scans, the Baseline model produced anatomically implausible segmentations on hydrocephalus cases. The Real-Paired model, although accurate on 3D T1w, failed on LR and other contrast inputs. Both **SynHydro** and **Real-Augmented** models yielded robust and anatomically consistent segmentation results across all tested conditions—healthy/hydrocephalus, pre-/post-operative, and varying modalities/resolutions—validating the effectiveness of the synthesized supervision and domain randomization.

Quantitative Segmentation Accuracy Here we report the DSC result (Table 1) on the annotated T1w test set. Consistent with the qualitative results, Real-Paired achieves the best performance on T1w, serving as an approximate upper bound. While the Baseline is slightly better on the control cohort, its performance drops substantially on the longitudinal cohort with hydrocephalus. **SynHydro** performs comparably to **Real-Augmented**, further demonstrating that our synthesized hydrocephalus data provides supervision nearly as effective as real pathological labels.

Cross-Modality Consistency (Volumetric Correlation) To evaluate robustness under heterogeneous imaging conditions, we computed tissue volumes from predictions on non-annotated modalities and LR scans and correlated them with volumes from the reference 3D T1w scans in Table 2. The Baseline

Table 2: **Consistency Evaluation Results.** Comparison of Pearson Correlation Coefficient (r, ↑) on Control and Longitudinal cohorts. The Longitudinal dataset is divided into Pre-operative and Post-operative phases.

Dataset	Method	Anatomical Structure						Avg.
		Ven_L	Ven_R	GM_L	GM_R	WM_L	WM_R	
Control	Baseline	0.936	0.863	0.938	0.954	0.889	0.855	0.906
	SynHydro (Ours)	0.974	0.913	0.940	0.923	0.849	0.826	0.904
	Real-Augmented	0.978	0.948	0.948	0.946	0.925	0.914	0.943
	Real-Paired	0.473	0.181	0.950	0.782	0.827	0.821	0.672
Longitudinal *Pre-operative*	Baseline	0.856	0.828	0.912	0.906	0.917	0.956	0.896
	SynHydro (Ours)	0.980	0.993	0.947	0.950	0.950	0.945	0.961
	Real-Augmented	0.990	0.993	0.941	0.937	0.972	0.979	0.969
	Real-Paired	0.734	0.829	0.932	0.909	0.920	0.924	0.875
Longitudinal *Post-operative*	Baseline	0.891	0.903	0.952	0.957	0.921	0.941	0.927
	SynHydro (Ours)	0.996	0.993	0.963	0.951	0.918	0.897	0.953
	Real-Augmented	0.996	0.993	0.947	0.898	0.962	0.961	0.959
	Real-Paired	0.805	0.859	0.904	0.898	0.818	0.842	0.854

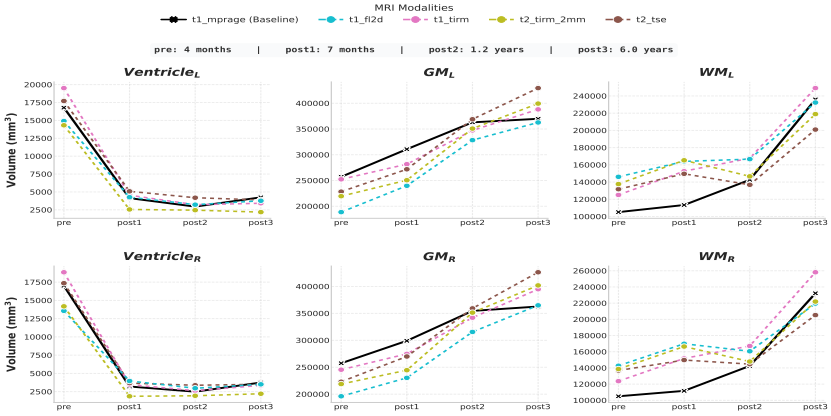

Fig. 3: Longitudinal cross-modality volume trajectories with SynHydro.

shows lower consistency due to the lack of hydrocephalus modeling. In contrast, both **SynHydro** and **Real-Augmented** models maintained high volumetric agreement, significantly outperforming the Real-Paired model, which generalized poorly to unseen modalities and resolutions. This confirms that the extensive domain randomization is crucial for cross-modality/cross-resolution robustness.

Pre- and Post-operative Volume Trajectory Following the quantitative validation, Fig. 3 presents a representative pre-/post-operative subject. Our method preserves coherent temporal trends across modalities, indicating robustness under varying acquisition settings. As shown, ventricular volume drops

markedly after surgery and then gradually increases with growth, while GM and WM volumes show a steady developmental recovery over time.

4 Conclusion

We presented SynHydro, a biomechanics-driven domain randomization framework for robust pediatric hydrocephalus segmentation. Please note that SynHydro is not a patient-specific biomechanical solver or a model for predicting the exact progression of hydrocephalus. Instead, it synthesizes a diverse set of hydrocephalus anatomies and multi-contrast MR images solely from healthy tissue labels, eliminating the need for scarce pathological annotations. Models trained exclusively on this synthetic data achieves segmentation performance comparable to models trained with real pathological labels. Crucially, SynHydro-trained models show superior generalization across MRI modalities, resolutions, and ages, and reliably capture critical clinical trends. SynHydro provides a practical solution to the annotation bottleneck, enabling the development of generalizable tools for quantitative hydrocephalus assessment.

Acknowledgments. This work was supported by the National Natural Science Foundation of China (Nos. T2522028 and 12326616), Natural Science Basic Research Program of Shaanxi (No. 2024JC-TBZC-09), and Shaanxi Provincial Key Industrial Innovation Chain Project (No. 2024SF-ZDCYL-02-10).

Disclosure of Interests. The authors have no competing interests to declare that are relevant to the content of this article.

References

1. Billot, B., Greve, D.N., Puonti, O., Thielscher, A., Van Leemput, K., Fischl, B., Dalca, A.V., Iglesias, J.E., et al.: Synthseg: Segmentation of brain mri scans of any contrast and resolution without retraining. Medical image analysis **86**, 102789 (2023)
2. Fischl, B.: Freesurfer. Neuroimage **62**(2), 774–781 (2012)
3. Hladky, S.B., Barrand, M.A.: Regulation of brain fluid volumes and pressures: basic principles, intracranial hypertension, ventriculomegaly and hydrocephalus. Fluids and Barriers of the CNS **21**(1), 57 (2024)
4. Hoffmann, M., Billot, B., Greve, D.N., Iglesias, J.E., Fischl, B., Dalca, A.V.: Synthmorph: learning contrast-invariant registration without acquired images. IEEE transactions on medical imaging **41**(3), 543–558 (2021)
5. Hoopes, A., Mora, J.S., Dalca, A.V., Fischl, B., Hoffmann, M.: Synthstrip: skull-stripping for any brain image. NeuroImage **260**, 119474 (2022)
6. Iglesias, J.E., Billot, B., Balbastre, Y., Magdamo, C., Arnold, S.E., Das, S., Edlow, B.L., Alexander, D.C., Golland, P., Fischl, B.: Synthsr: A public ai tool to turn heterogeneous clinical brain scans into high-resolution t1-weighted images for 3d morphometry. Science advances **9**(5), eadd3607 (2023)

7. Isensee, F., Jaeger, P.F., Kohl, S.A., Petersen, J., Maier-Hein, K.H.: nnu-net: a self-configuring method for deep learning-based biomedical image segmentation. Nature methods **18**(2), 203–211 (2021)
8. Jenkinson, M., Beckmann, C.F., Behrens, T.E., Woolrich, M.W., Smith, S.M.: Fsl. Neuroimage **62**(2), 782–790 (2012)
9. Jinbo, H., Iwamoto, Y., Nonaka, M., Chen, Y.W.: Automatic segmentation of infant brain ventricles with hydrocephalus in mri based on deep multi-path learning. In: 2022 IEEE International Conference on Consumer Electronics (ICCE). pp. 1–4. IEEE (2022)
10. Kahle, K.T., Klinge, P.M., Koschnitzky, J.E., Kulkarni, A.V., MacAulay, N., Robinson, S., Schiff, S.J., Strahle, J.M.: Paediatric hydrocephalus. Nature reviews Disease primers **10**(1), 35 (2024)
11. Klimont, M., Flieger, M., Rzeszutek, J., Stachera, J., Zakrzewska, A., Jończyk-Potoczna, K.: Automated ventricular system segmentation in paediatric patients treated for hydrocephalus using deep learning methods. BioMed research international **2019**(1), 3059170 (2019)
12. Krishnamurthy, S., Li, J.: New concepts in the pathogenesis of hydrocephalus. Translational pediatrics **3**(3), 185 (2014)
13. Largent, A., De Asis-Cruz, J., Kapse, K., Barnett, S.D., Murnick, J., Basu, S., Andersen, N., Norman, S., Andescavage, N., Limperopoulos, C.: Automatic brain segmentation in preterm infants with post-hemorrhagic hydrocephalus using 3d bayesian u-net. Human brain mapping **43**(6), 1895–1916 (2022)
14. Leinonen, V., Vanninen, R., Rauramaa, T.: Cerebrospinal fluid circulation and hydrocephalus. Handbook of clinical neurology **145**, 39–50 (2018)
15. Maeda, H., Iwamoto, Y., Nonaka, M., Li, Y., Chen, Y.W.: A multi-view weighted fusion model for segmentation of infant brain ventricles with hydrocephalus in mri. In: 2023 IEEE 12th Global Conference on Consumer Electronics (GCCE). pp. 727–730. IEEE (2023)
16. O'hayon, B., Drake, J.M., Ossip, M., Tuli, S., Clarke, M.: Frontal and occipital horn ratio: a linear estimate of ventricular size for multiple imaging modalities in pediatric hydrocephalus. Pediatric neurosurgery **29**(5), 245–249 (1998)
17. Pérez-García, F., Sparks, R., Ourselin, S.: Torchio: a python library for efficient loading, preprocessing, augmentation and patch-based sampling of medical images in deep learning. Computer methods and programs in biomedicine **208**, 106236 (2021)
18. Qiao, Y., Tao, H., Huo, J., Shen, W., Wang, Q., Zhang, L.: Robust hydrocephalus brain segmentation via globally and locally spatial guidance. In: International Workshop on Machine Learning in Clinical Neuroimaging. pp. 92–100. Springer (2021)
19. Sobana, M., Halim, D., Aviani, J.K., Gamayani, U., Achmad, T.H.: Neurodevelopmental outcomes after ventriculoperitoneal shunt placement in children with non-infectious hydrocephalus: a meta-analysis. Child's Nervous System **37**(4), 1055–1065 (2021)
20. Tierney, T.M., Alexander, N.A., Avila, N.L., Balbastre, Y., Barnes, G., Bezsudnova, Y., Brudfors, M., Eckstein, K., Flandin, G., Friston, K., et al.: Spm 25: open source neuroimaging analysis software. arXiv preprint arXiv:2501.12081 (2025)
21. Vinchon, M., Rekate, H., Kulkarni, A.V.: Pediatric hydrocephalus outcomes: a review. Fluids and Barriers of the CNS **9**(1), 18 (2012)
22. Wang, L., Wu, Z., Chen, L., Sun, Y., Lin, W., Li, G.: ibeat v2. 0: a multisite-applicable, deep learning-based pipeline for infant cerebral cortical surface reconstruction. Nature protocols **18**(5), 1488–1509 (2023)

23. Wang, Y., Liu, Y., Wei, S., Xue, Y., Zuo, L., Remedios, S.W., Bian, Z., Meggyesy, M., Ahn, J., Lee, R.P., et al.: Deep-learning-based segmentation of hydrocephalus brain ventricle from ultrasound. In: Medical Imaging 2024: Image Processing. vol. 12926, pp. 789–794. SPIE (2024)
24. Xu, Y., Ding, Y., Sun, H., Zhang, H., Zhao, L.: Hykid: An open mri dataset with expert-annotated multi-structure and choroid plexus in pediatric hydrocephalus. arXiv preprint arXiv:2509.19218 (2025)
25. Yang, Q., Huang, K., Zhang, G., Li, X., Gao, Y., Zhao, C.: Relationship between the volume of ventricles, brain parenchyma and neurocognition in children after hydrocephalus treatment. Child's Nervous System **41**(1), 48 (2025)
26. Zhang, A., Khan, A., Majeti, S., Pham, J., Nguyen, C., Tran, P., Iyer, V., Shelat, A., Chen, J., Manjunath, B.: Automated segmentation and connectivity analysis for normal pressure hydrocephalus. BME frontiers **2022**, 9783128 (2022)
27. Ziegelitz, D., Hellström, P., Björkman-Burtscher, I.M., Agerskov, S., Stevens-Jones, O., Farahmand, D., Tullberg, M.: Evaluation of a fully automated method for ventricular volume segmentation before and after shunt surgery in idiopathic normal pressure hydrocephalus. World neurosurgery **181**, e303–e311 (2024)
28. Zöllei, L., Iglesias, J.E., Ou, Y., Grant, P.E., Fischl, B.: Infant freesurfer: An automated segmentation and surface extraction pipeline for t1-weighted neuroimaging data of infants 0–2 years. Neuroimage **218**, 116946 (2020)